Scattering Characteristic Extraction and Recovery for Multiple Targets Based on Time Frequency Analysis

Xiangwei Liu [1], Jianzhou Li [1], Yi Zhu [1], and Shengjun Zhang [2]

[1] School of Electronics and Information
Northwestern Polytechnical University, Xi'an, 710129, China
lxw1218@mail.nwpu.edu.cn, ljz@nwpu.edu.cn, 958637071@qq.com

[2] National Key Laboratory of Science and Technology on Test Physics & Numerical Mathematical
Beijing, 100076, China
Zhangsj98@sina.com

Abstract ─ The multi-target scattering field consists of the scattering fields of each target, but it is difficult to know the scattering characteristics of the specific target from the total scattering field. However, the scattering characteristics of single target embedded in the total scattered field have important research significance for target recognition and detection. In this paper, a method is proposed to extract and recover each target's scattering characteristics from the total scattering field of multiple targets. The theoretical basis of the method is that the scattering echoes corresponding to different targets reach the receiver at different time. We acquire the total scattering field at first. Then, we perform the signal processing with time-frequency analysis to obtain the arrival time of different scattering echoes. According to the time slot difference, the time domain signal of each target can be extracted to recover its scattering field. Several examples validate the proposed method.

Index Terms ─ Extraction and recovery, radar detection, scattering characteristic, time-frequency analysis.

I. INTRODUCTION

Since the scattering field of multi-target is redundant and aliased, it is very difficult to obtain the individual scattering characteristics of each target from the total scattering field. However, the scattering characteristic of each target is of great significance for target recognition and radar detection [1-4]. In this paper, we extract and recover scattering characteristics from the total scattering field with time-frequency analysis. Time-frequency analysis is used in [5] and [6] to process radar imaging to reduce multiple scattering and clutter in radar images, based on the principle that different scattering echoes have different resolutions. Time-frequency analysis is also used in [7] to process the target's scattering field to suppress the scattering centers caused by the coupling effect in radar imaging. All of them have used time-frequency analysis only to improve the probability of radar recognition. [8] uses the linear frequency-modulated continuous-wave radar system and Gabor-Wigner transform to realize the recognition of multiple targets, which realizes the detection of the number of multiple targets. [9] also uses linear frequency-modulated continuous-wave radar system to achieve the detection of the speed and distance of each target in multiple targets. In the field of multi-target detection, the existing work is mostly to design radar detection systems or methods to improve the detection efficiency and accuracy of multiple targets [10-14], which mainly detects the number, speed, and direction. [15-17] use image processing methods to extract the scattering center in radar imaging, and use the extracted scattering center to rebuild the local scattering characteristics of the target. They depend on the radar images of the target and cannot extract and recovery the scattering characteristics of the target through only one-dimensional data. In this paper, we focus on extracting and recovering the individual scattering characteristics of each target from the multi-target's total scattering field, which has very great significance for multi-target recognition.

The paper is organized as follows. In Section II, we introduce the theoretical basis of the method and its numerical realization. In Section III, some results are presented, and we use specific examples to illustrate how to extract the scattering field. Some conclusions are made in Section IV.

II. EXTRACTION AND RECOVERY FORMULATIONS

In this section, we represent the theory and the process of the extraction and recovery method. In multiple target scattering case, times for scattering echoes of different targets to reach the receiver are

different. However, when the distance between two targets is very close, it is difficult to distinguish the time difference in testing, so the scattering field received by the radar is usually the total scattering field, i.e., the mixed scattering field of multiple targets. However, this time slot difference can be used to achieve the extraction and recovery of the scattering characteristics of different targets from the total scattered field in simulation. For instance, the distance between the i-th target and the radar is D_i, and the time from the electromagnetic wave being transmitted to it being received by the radar is $T_i = 2D_i/c$, where c is the speed of light in free space. There is a time slot difference ΔT_i between the times when the scattering echoes from different targets reach the radar:

$$\Delta T_i = 2\left|\frac{D_i - D_{i+1}}{c}\right|. \tag{1}$$

The total scattered E field E_s of multiple targets is obtained by calculation or experiment.

We perform Short-Time Fourier Transform (STFT) [18] on the scattering field E_s to obtain the time difference, which is defined as (2):

$$STFT_s(t,\omega) = \int_{-\infty}^{+\infty} E_s(\tau)h(\tau-t)e^{-j\omega\tau}d\tau. \tag{2}$$

The window function $h(t)$ is a Kaiser window in (2), which is defined as (3):

$$h(n) = \begin{cases} \dfrac{J_0\left[\beta\sqrt{1-(2n/N)}\right]}{J_0(\beta)}, |n| < \dfrac{N}{2}, n = -\dfrac{N}{2} \\ 0 \qquad\qquad ,|n| > \dfrac{N}{2}, n = \dfrac{N}{2} \end{cases}, \tag{3}$$

where J_0 is 0th-order Bessel function of the first kind, n and N are the width of the window function and the length of the signal, respectively. β is a parameter used to adjust the performance of the window function.

Afterwards, the time domain signal $R(t)$ consisting of multiple peaks at ω_i in $STFT_s(t,\omega)$ is extracted:

$$R(t)\big|_{\omega=\omega_i} = STFT_s(t,\omega). \tag{4}$$

$R(t)$ is a time-domain signal composed of multiple peaks, we can simplify it as (5) and the times corresponding to different peaks are the time when the scattering signal of different targets are received:

$$\begin{aligned}R(t) = P(\Delta t_1) + P(\Delta t_2) + \cdots \\ + P(\Delta t_i) + \cdots + P(\Delta t_l)\end{aligned}, \tag{5}$$

where $P(\Delta t_i)$ is the peak occupying the time period of Δt_i, l is the number of peaks that $R(t)$ has.

Since the scattering echo of a scatterer may correspond to multiple peaks, the group delay processing,

defined as (6), is performed on the scattering field before STFT for better observing the time slot difference [15]:

$$E_s' = E_s \bullet e^{-j2\pi f_i d}, \tag{6}$$

where d is the group delay time, and E_s' is the scattering data obtained after group delay processing.

We extract the $P(\Delta t)$s, which is the set of peaks belonging to the same scatterer from $R(t)$, and fill them with zero at the default time, so that the length of the reconstructed signal $R'(t)$:

$$R'(t) = P(\Delta t)s + Z(t-\Delta t), \tag{7}$$

and remain the same with $R(t)$. In (7), $Z(t-\Delta t)$ is the zero signal at the occupied time of other peaks. For the time-domain signal, there is no good way to identify different scatterers correspond to each peak in $R(t)$. However, in principle, we can distinguish each peak in this way. The larger the amplitude of the peak, the earlier the corresponding scattering echo reaches the receiver, since the EM wave is continuously attenuated during the propagation. And, the larger the peak, the larger the volume of the corresponding scatterer.

Finally, the extracted scattering signals are reconstructed with the Inverse Short-Time Fourier Transform (ISTFT) defined as (8) [18]. Thus, the scattered fields of each target in multiple targets can be recovered:

$$S(t) = \frac{1}{2\pi} \int_{-\infty}^{+\infty}\int_{-\infty}^{+\infty} STFT_s(\omega,\tau)e^{j\omega t}d\omega d\tau. \tag{8}$$

The steps of extraction and recovery of scattering characteristics mainly include (see Fig. 1).
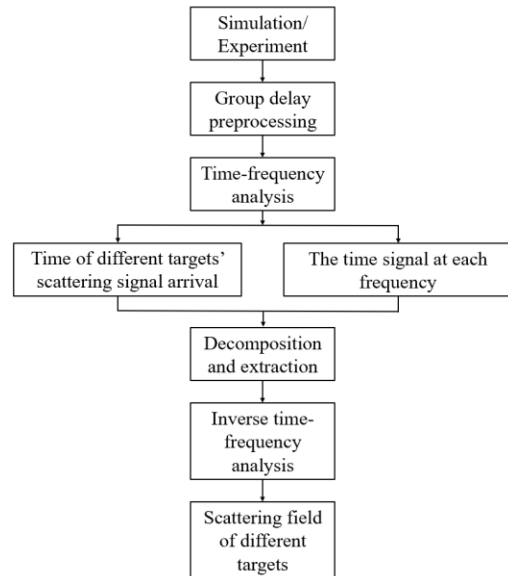
Fig. 1. The steps of extraction and recovery of scattering characteristics.

The range resolution $\Delta r = c/2B$ needs to meet certain conditions. Where B is the frequency bandwidth. Firstly, the resolution needs to be smaller than the size of the target. If the resolution is larger than the size of the target, we cannot observe the scattering echo corresponding to the target in the time-domain signal. Secondly, the resolution also needs to be smaller than the distance between the targets. This is because when the resolution is greater than the separation between objects, the scattering echoes of different objects in the time-domain signal will overlap, which is not conducive to the extraction and recovery of their scattering characteristics.

III. NUMERICAL EXAMPLES

In this section, we explain in detail the method for extraction and recovery of the scattering characteristics through several examples. The incident wave in the paper is horizontally polarized.

A. Double PEC spheres

Firstly, we use double-PEC spheres shown in Fig. 2 to specifically explain the application of this algorithm for scattering characteristic extraction and recovery of different targets. The diameter of the big ball is 1m, and the diameter of the small ball is 0.1m. The Shooting and Bouncing Ray (SBR) algorithm is used to calculate their scattering field [19-20]. The incident direction is $\theta = 20°, \varphi = 0°$, where θ is the angle between the incident wave and z axis, φ is the angle between the projection of the incident wave on the xoy plane and x axis, and the frequency is from 3GHz to 6 GHz, with 0.05 GHz interval, and the range resolution $\Delta r = 0.05m$ is smaller than the diameter of the small sphere. The radar cross section (RCS) is shown in Fig. 3.
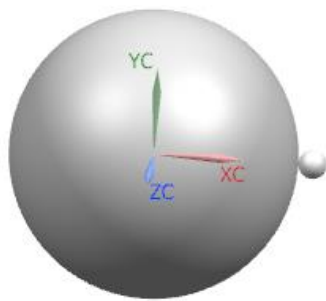
Fig. 2. The double PEC spheres.

Then, group delay is performed on the scattering field to obtain E_s', where $d = 9 \times 10^{-9}$s. Afterwards, we perform the STFT on the E_s' with $n = 61, \beta = 6$, and these parameters are designed to maximize the resolution of time-frequency analysis.
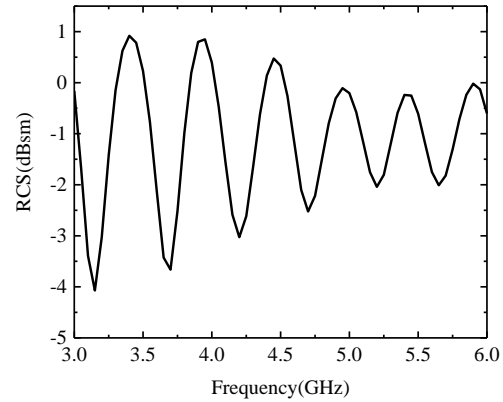
Fig. 3. The RCS of double PEC spheres.

The time-frequency analysis result is shown in Fig. 4 (a). In addition to the two strong scattering echoes, there are obvious smears in Fig. 4 (a). The scattering of the big sphere produces the strongest scattering echo, and the scattering of the small one corresponds to the second strong echoes, while the multiple scattering between the double spheres produces weaker scattering echo and smears [21].

(a)

(b)
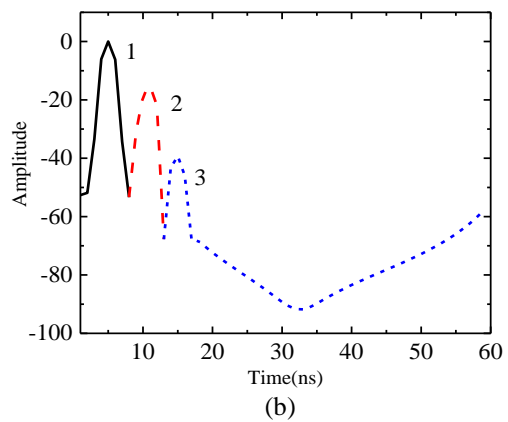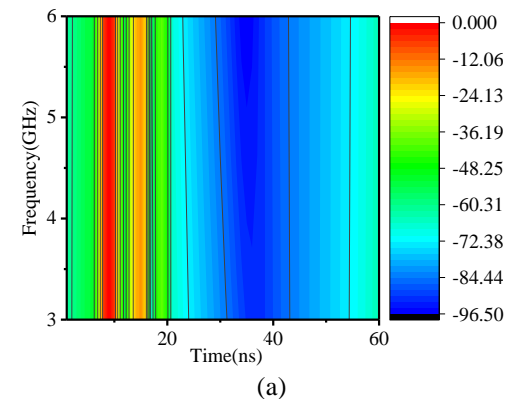
Fig. 4. The time domain signal extracted from the time-frequency result. (a) The time-frequency analysis result, and (b) the extracted time domain signal.

We extract the time domain signal $R(t)$ from the time-frequency analysis result at 6GHz, which is shown in Fig. 4 (b). In $R(t)$, there are three peaks, and they can be decomposed according to the time occupied by themselves. The peak1 indicates the time when the echo by the big sphere reaches the radar, the peak2 is occupied by the small sphere, and the peak3 occupies the time of multiple scattering echoes between the two spheres reaching the radar. When the range resolution cell contains different scatterers, these corresponding scattering echo will be mixed together and appear in the same peak of the time domain signal. Therefore, after we extract the scattering field of such peak in $R(t)$, the extracted scattering field will contain the fore mentioned multiple scatterers' scattering characteristics, and this will cause the extraction and recovery failure in this case.

We do the same for every time domain signals in the time-frequency analysis result. After that, it's necessary to extend the length of extracted signals to N by 'zero padding', and then they are processed with ISTFT to obtain the scattering characteristics corresponding to different targets.

We calculate the scattering field of the big sphere by SBR with the same parameters, and compare the calculated scattering field with the extracted one to verify the validity of the recovered scattered field.

The RCSs of the double spheres and the large sphere are shown in Fig. 5. In Fig. 5, due to the existence of the small sphere, the RCSs of the double-PEC spheres and the large sphere are quite different, with a maximum difference of nearly 3dB. The recovered RCS of the large sphere and its calculated RCS are in good agreement from 3.1GHz to 5.8GHz, which shows that peak1 corresponds to the scattering field of the large sphere. Since the side lobe of the window function $h(t)$ used in

STFT is large, so they do not match well at both ends of frequency. This can be improved by using different window functions.
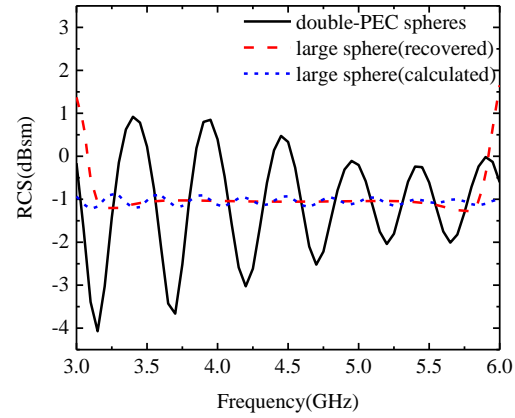
Fig. 5. The comparison of RCSs.

Calculate the scattering E field of the double PEC spheres from $\theta = 20°, \varphi = 180°$ to $\theta = 20°, \varphi = 0°$ with $0.67°$ interval, and the frequency from 3 GHz to 6GHz, with 0.05 GHz interval, and the radar image of the double PEC spheres is shown in Fig. 6 (a), in which there are two scattering centers according to different spheres [22-23]. It is easy to know that the scattering center located at (20,20) corresponds to the large sphere and the scattering field of the small sphere forms the scattering center located at (20,30).

Similarly, we perform the decomposition process on the scattering field at every angle, and image the extracted and recovered scattering fields individually as shown in Figs. 6 (b) and (c). The scattering E fields of the large sphere and the small sphere are recovered well.
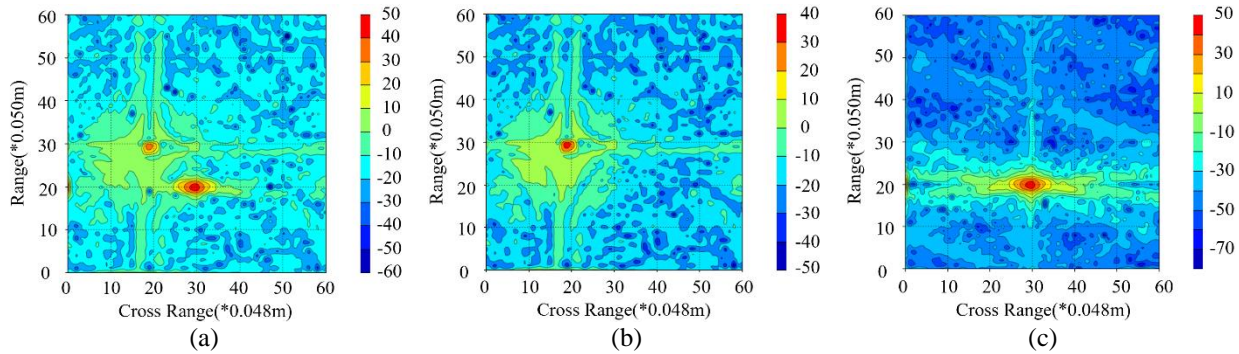
Fig. 6. The radar images of different spheres (calculated and recovered). (a) The double PEC spheres (calculated), (b) the small PEC sphere (recovered), and (c) the big PEC sphere (recovered).

B. Plane with corner reflector

A plane can disguise its own scattering characteristic by emitting a corner reflector as shown in the Fig. 7. Here a plane about 16m long and 10m meters wide, and a 1.5m corner reflector, are shown in Fig. 7. The SBR algorithm is used to calculate the scattering E field at $\theta = 0°, \varphi = 0°$,

and the frequency is from 1.5GHz to 4.5 GHz, with 0.005 GHz interval. The RCS is shown in Fig. 8.
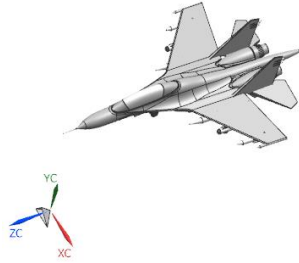
Fig. 7. Plane with corner reflector
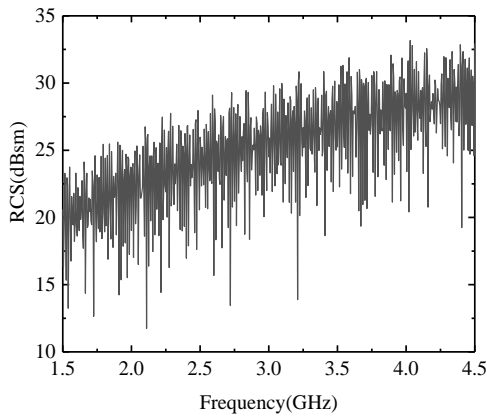
Fig. 8. The RCS of the plane with corner reflector.

The scattering E field is recovered according to the proposed method. In order to verify the accuracy of the recovered field, the RCS of the plane without the corner reflector is calculated with the same calculating

parameters. The calculated and recovered RCSs of the plane are shown in Fig. 9.
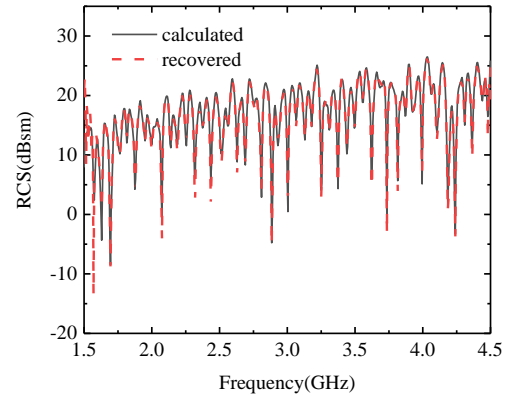
Fig. 9. The calculated and recovered RCSs of the plane.

The two RCS curves in Fig. 9 match very well, which demonstrates that the scattering characteristic of the plane is well recovered and the influence of the corner reflector is eliminated.

Similarly, we calculate the radar image of the plane with the corner reflector, which is shown in Fig. 10 (a). The angle range is form $\theta = -30°, \varphi = 0°$ to $\theta = 30°, \varphi = 0°$, with $0.1°$ interval, and the frequency is from 1.5GHz to 4.5GHz, with 0.005 GHz interval.

In Fig. 10 (a), the scattering center located at (300,300) is generated by the corner reflector and the scattering centers located at upper area correspond to the plane. Figures 10 (b) and (c) are the radar images of the recovered scattering fields of the plane and the corner reflector respectively, which demonstrate the total scattering filed is decomposed well.
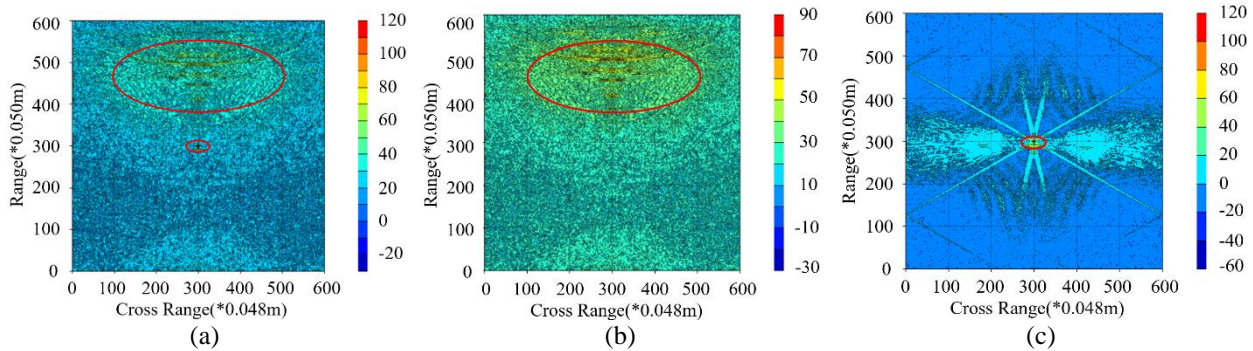
Fig. 10. The radar images of plane and corner reflector (calculated and recovered). (a) Plane with corner reflector (calculated), (b) plane without corner reflector (recovered), and (c) corner reflector (recovered).

C. Target array

As shown in Fig. 11, three types of targets form a target array. The space occupied by the target array is approximately $9\text{m} \times 11\text{m}$.

The SBR algorithm is used to calculate the scattering field of the target array at $\theta = -30°, \varphi = 0°$, and the frequency is from 1.5GHz to 4.5 GHz, with 0.01 GHz interval. The result is shown in Fig. 12.
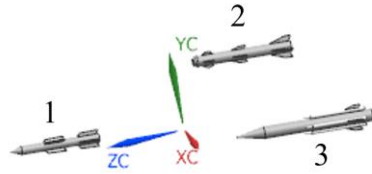
Fig. 11. The target array.
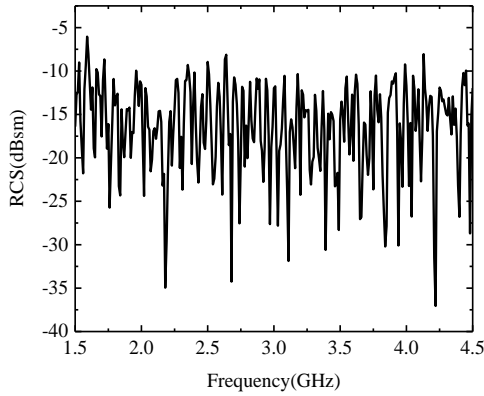
Fig. 12. The RCS of the target array.

We process the total scattering field to recover the scattering fields of each targets. Simultaneously, we calculate the scattering characteristics of each targets separately, and compare the recovered results with the calculated ones as shown in Fig. 13. The respective comparison of target 1 and target 2 are very consistent, indicating that their scattering fields recovered from the total scattering field are very accurate.

However, there is a significant difference between the calculated and the recovered RCS of target 3 in Fig. 13 (c). This is because part of target 3 is blocked by target 1 at $\theta = -30°, \varphi = 0°$, which is quite different from the calculated result in which there is no shielding effect from other object.
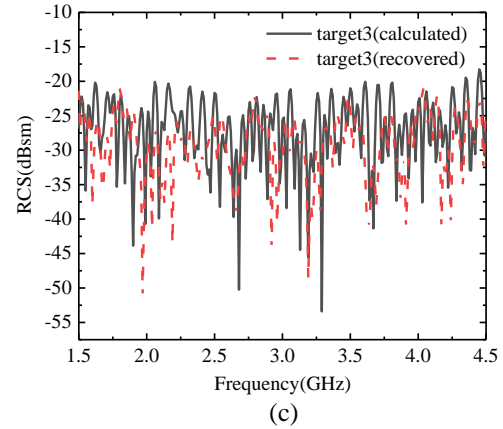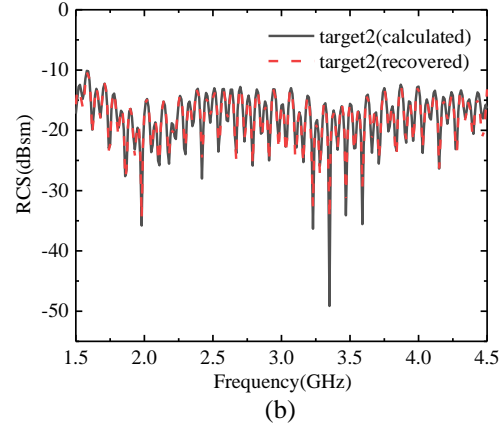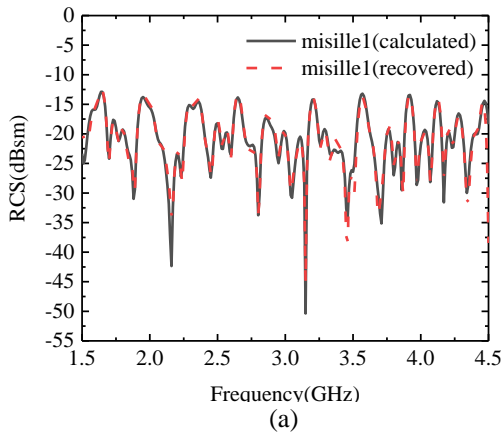
Fig. 13. The calculated and recovered RCSs of each target: (a) target 1, (b) target 2, and (c) target 3.
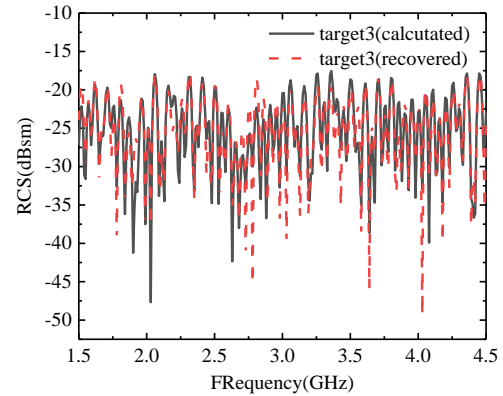
Fig. 14. The calculated and recovered RCSs of target 3 at $\theta = 30°, \varphi = 0°$.

In order to verify such analysis, we recalculate the scattering fields of the target array and target 3 respectively at $\theta = 30°, \varphi = 0°$, and the recovered and calculated RCSs of target 3 are shown in the Fig. 14, which shows good agreement. Therefore, to recover the

true scattering characteristics of each target in target array, it is necessary to obtain scattering fields at multiple angles to prevent the target from being shadowed.

D. The test double-PEC spheres

The double-PEC spheres as shown in Fig. 15 are measured in a chamber to obtain the scattering field. The large metal sphere has a diameter of 300mm. The small metal sphere has a diameter of 116mm. The distance between the two spheres is 38mm. The angular is from $\theta = 20°, \varphi = 180°$ to $\theta = 20°, \varphi = 0°$, with 1° interval, and the frequency is from 6GHz to 12GHz, with 0.15GHz interval, and the measured radar image of the test double-PEC sphere is shown in Fig. 16.

Fig. 15. The test double-PEC spheres.

In Fig. 16, there are three scattering centers. The scattering center at (13,15) is formed by the scattering of the large sphere, while the scattering field of small sphere forms the scattering center at (22,18). The scattering center at (20,20) is caused by multiple scattering between the double spheres [24]. Despite the interference of multiple scattering, the proposed method can still effectively extract and recovery the scattering characteristics of each sphere.
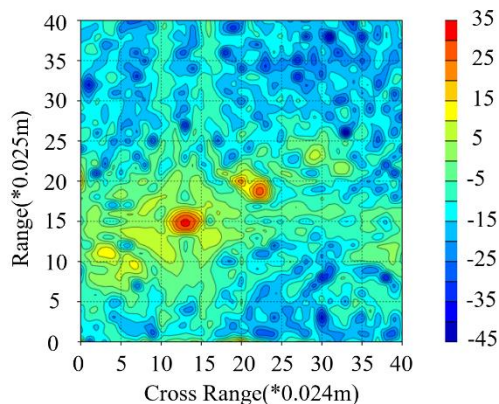
Fig. 16. The radar image of the test double-PEC spheres.

We use the proposed method to deal with the measured scattering field of the double spheres, and extract and recover the scattering fields of the large and

small spheres respectively from the total scattering field. Because the scattering mechanism contained in the measured scattering field is more complicated than the calculated one, we directly image the extracted scattering field to observe whether the scattering field has been accurately extracted and recovered.

The recovered scattering fields of the large and small spheres are imaged as shown in Figs. 17 (a) and (b) respectively, which shows that the double spheres' total scattering field is well decomposed, and we have completely extracted the large and small spheres' scattering fields from it, and accurately recovered their scattering characteristics.
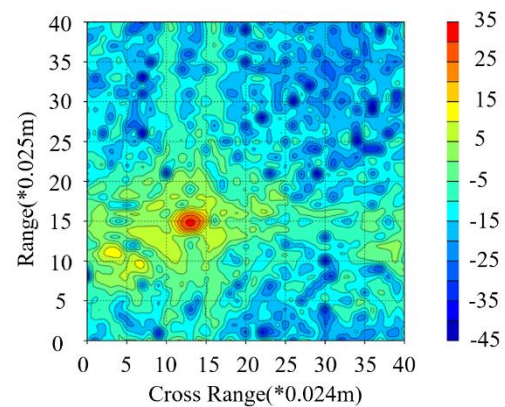
(a)
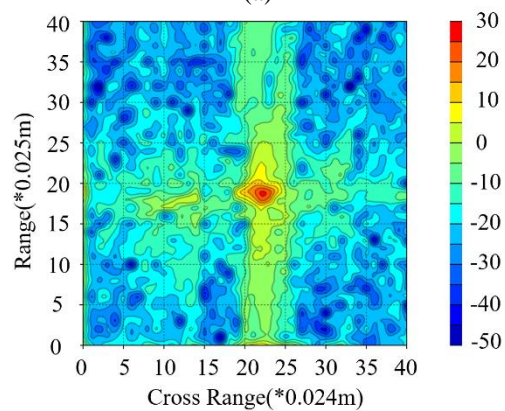
(b)

Fig. 17. The rebuild radar images: (a) the large sphere, and (b) the small sphere.

In addition, we extract multiple scattering from the total scattering field, which is imaged in Fig. 18. Extracting different scattering mechanisms from the total scattering field is also of great significance for deep understanding and further controlling of the scattering characteristics, and has a wide range of applications in radar detection such as to improve the accuracy in the target recognition based on radar image.
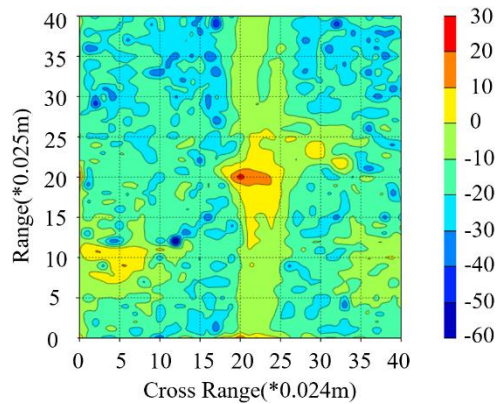
Fig. 18. The radar image of the multiple scattering.

VI. CONCLUSION

In this paper, we extract and recover the scattering characteristics from the total scattered filed of multiple targets based on time-frequency analysis to determine the time of each scattering echoes arrival. For the double PEC spheres, the plane with corner reflector, the target array, and the test double PEC spheres, their scattering characteristics are well recovered, indicating that the proposed method is very useful for scattering field decomposition, and is also of great significance for complex target's electromagnetic scattering cognition and feature recognition.

ACKNOWLEDGMENT

REFERENCES

[1] B. Y. Ding, G. J. Wen, X. H. Huang, J. R. Zhong and C. H. Ma, "Target recognition in SAR images via Gaussian mixture modeling of attributed scattering center set," *2016 CIE International Conference on Radar*, Guangzhou, China, Oct. 10-13, 2016.

[2] S. R. Cloude and E. Pottier, "A review of target decomposition theorems in radar polarimetry," *IEEE Transactions on Geoscience and Remote Sensing*, vol. 34, no. 2, pp. 498-518, 1996.

[3] S. P. Xiao, G. R. Guo, Z. W. Zhuang, and M. Y. Luo, "Radar target modeling and recognition based on scattering centers," *Proceedings of National Aerospace and Electronics Conference*, Dayton, OH, USA, May 23-27, 1994.

[4] D. F. Fuller, "Phase History Decomposition for efficient Scatterer Classification in SAR Imagery," *Dissertations & Theses - Gradworks*, vol. 4, no. 8, pp. 921-922, 2011.

[5] E. Giusti, M. Martorella, and A. Capria, "Polarimetrically persistent scatterer based automatic target recognition," *IEEE Transactions on Geoscience and Remote Sensing*, vol. 49, no. 11, pp. 4588-4599, 2011.

[6] T. T. Feng, L. X. Guo, and Y. Zhang, "Inverse synthetic aperture radar imaging of maneuvering targets based on joint time-frequency analysis," *2016 IEEE International Geoscience and Remote Sensing Symposium*, Beijing, China, 2016.

[7] M. Q. Ren and Y. H. Tian, "Radar signal cognition based on time-frequency transform and high order spectra analysis," *2017 IEEE International Conference on Signal Processing, Communications and Computing*, Xiamen, China, 1-4, 2017.

[8] C. Özdemir, *Inverse Synthetic Aperture Radar Imaging with MATLAB Algorithms*. John Wiley & Sons Inc., 2012.

[9] L. Su, H. S. Wu, and C. C. Tzuang, "2-D FFT and time-frequency analysis techniques for multi-target recognition of FMCW radar signal," *Asia-Pacific Microwave Conference 2011*, Melbourne, VIC, USA, Dec. 5-8, 2011.

[10] W. Z. Yan, F. W. Kong, and P. C. Hu, "Algorithm and DSP design of LFMCW radar for multiple," *2018 National Microwave Millimeter Wave Conference*, Chengdu, China, 6, May 2018.

[11] Y. Z. Fan, Z. L. Yang, and X. Y. Bu, "Radar waveform design and multi-target detection in vehicular applications," *2015 International Conference on Estimation, Detection and Information Fusion (ICEDIF)*, Harbin, China, Jan. 10-11, 2015.

[12] L. H. Fan, Y. M. Pi, and S. J. Huang, "Multi-target imaging processing algorithms of ISAR based on time-frequency analysis," *2006 CIE International Conference on Radar*, Shanghai, China, Oct. 16-19, 2006.

[13] P. C. Guo, Z. Liu, and J. J. Wang, "HRRP multi-target recognition in a beam using prior-independent DBSCAN clustering algorithm," *IET Radar, Sonar & Navigation*, vol. 13, no. 8, pp. 1366-1372, 2019.

[14] H. Jiang, X. H. Tang, W. Lv, and Y. Li, "Blind multi-target detection for bistatic MIMO radar based on random matrix theory," *2015 IEEE China Summit and International Conference on Signal and Information Processing*, Chengdu, China, July 12-15, 2015.

[15] J. Z. Li, C. Q. Fan, L. Liu, W. Z. Wang, and X. Y. Wang, "Radar target characteristic extraction and rebuilding of multi-target based on scattering center," *2017 Sixth Asia-Pacific Conference on Antennas and Propagation (APCAP)*, Xi'an, China, 2017.

[16] S. Cui, S. Li, and H. Yan, "A method of 3-D scattering center extraction based on ISAR images," *2016 IEEE International Conference on Electronic Information and Communication Technology (ICEICT)*, Harbin, China, 2016.

[17] Y. S. Lin, L. Zhang, A. K. Xue, D. Peng, and Z. Jin, "SAR imagery scattering center extraction and target recognition based on scattering center model," *2006 6th World Congress on Intelligent Control and Automation*, Dalian, China, 2006.

[18] S. Qian, *Introduction to Time-Frequency and Wavelet Transforms*. China Machine Press, 2005.

[19] T. Q. Fan, L. X. Guo, B. Lv, W. Liu, "An improved backward SBR-PO/PTD hybrid method for the backward scattering prediction of an electrically large target," *IEEE Antennas and Wireless Propagation Letters*, vol. 15, pp. 512-515, 2016.

[20] Y. An, Z. Fan, D. Ding, and R. Chen, "FPO-based shooting and bouncing ray method for wide-band RCS prediction," *The Applied Computational Electromagnetics Society Journal*, vol. 29, no. 4, 2014.

[21] S. M. Yucedag and A. Kizilay, "Time domain analysis of ultra-wide band signals from buried objects under flat and slightly rough surfaces," *The Applied Computational Electromagnetics Society Journal*, vol. 28, no. 8, 2013.

[22] K. T. Kim amd H. T. Kim, "Two-dimensional scattering center extraction based on multiple elastic modules network," *IEEE Transactions on Antennas and Propagation*, vol. 51, no. 4, pp. 848-861, 2003.

[23] B. Y. Ding, G. J. Wen, X. Huang, C. Ma, and X. Yang, "Target recognition in synthetic aperture radar images via matching of attributed scattering centers," *IEEE Journal of Selected Topics in Applied Earth Observations and Remote Sensing*, vol. 10, no. 7, pp. 3334-3347, 2017.

[24] J. Z. Li and X. W Liu, "Decomposition of scattering mechanisms based on time slot difference," *Systems Engineering and Electronics*, vol. 42, no. 3, pp. 513-520, 2020.

Xiang-Wei Liu is currently pursuing Master in Electromagnetic Fields and Microwave at Northwestern Polytechnical University. His current research direction is target electromagnetic scattering decomposition, target scattering characteristics evaluation and complex target modeling.

Jian-Zhou Li is an Associate Professor in Northwestern Polytechnical University. He received the Ph.D. degree in 2005 in Northwestern Polytechnical University. He was a postdoctoral researcher at University of Surrey during 2008-2009. His research interests focus on electromagnetic modeling and simulation.

Yi Zhu is currently pursuing Master in Electromagnetic Fields and Microwave at Northwestern Polytechnical University. His current research direction is electromagnetic calculation of dielectric coating target and complex target modeling.

Sheng-Jun Zhang is a Researcher in National Key Laboratory of Science and Technology on Test Physics & Numerical Mathematical, and his research direction is target feature control technology.